Struvite-K crystal growth inhibition by citric acid: formation of complexes in solution and surface adsorption effects.

Alberto Viani[a,*], Lucie Zárybnická[a], Radek Ševčík[a], Petra Mácová[a], Jana Machotová[b], Kateřina Veltruská[c]

[a]Institute of Theoretical and Applied Mechanics of the Czech Academy of Sciences, Centre Telč, Prosecká 809/76, 190 00 Praha 9, Czech Republic.

[b]Institute of Chemistry and Technology of Macromolecular Materials, Faculty of Chemical Technology, University of Pardubice, Studentská 573, 532 10 Pardubice, Czech Republic

[c]Department of Surface and Plasma Science, Faculty of Mathematics and Physics, Charles University, V Holešovičkách 2, 180 00 Prague 8, Czech Republic

*Corresponding author: Alberto Viani, e-mail: viani@itam.cas.cz;

Full mail address: Institute of Theoretical and Applied Mechanics of the Czech Academy of Sciences, Centre Telč, Batelovská 485, CZ-58856 Telč, Czech Republic.

Tel. +420 567225308.

Abstract

Controlled precipitation of struvite-K is of interest in the treatment of kidney stones, for phosphorous and potassium recovery from wastewaters, and in the chemistry of magnesium phosphate cements. The effect of citric acid in the growth of struvite-K from solution has been studied at room temperature and pH = 9 under different conditions of energy of mixing and

concentrations of the reactants. The time-evolution of pH during the precipitation reaction evidenced that the citric acid increased induction time and decreased the apparent growth rates of crystals. Chemical speciation analysis, measurements of citrate concentration, zeta potential and X-ray photoelectron spectroscopy indicated that crystallization is controlled by the formation of complexes with magnesium ions in solution and adsorption of citric acid at the growing surfaces. In analogy with Ca-carbonates and Ca-phosphates, the latter process impairs formation of nuclei of critical size. Crystal habit is dictated by supersaturation conditions and selective adsorption at crystal faces in reason of their residual charge density; consequently, alteration in the crystal shape is observed, and the average size of crystals and the amount of precipitate are reduced.

Keywords: struvite-k; citric acid; nucleation; X-ray photoelectron spectroscopy; zeta potential; magnesium phosphate cements.

---

1. Introduction

Struvite and struvite-K ($MgNH_4PO_4 \cdot 6H_2O$ and $MgKPO_4 \cdot 6H_2O$, respectively), are components of the so-called infectious urinary (kidney) stones. Their precipitation occurs when the urinary tract is colonized by bacteria. The growth of stones can have serious consequences as it is frequently associated with a renal tissue damage (Mclean et al., 1988).

Precipitation can also occur on pipe walls and equipment of the wastewater treatment industry; the formed scale deposits are the cause of significant problems (Mohajit et al., 1989).

On the other hand, crystallization of phosphates has been devised as a sustainable and economical method for phosphorus recovery from wastewaters and from ashes of biomass combustion (Gao et al., 2018). In fact, this method is adopted to compensate for the increasing demand for phosphorus and mitigate the exploitation of phosphate rock deposits (Shaddel et al., 2020).

In these different contexts, there is interest in controlling/inhibiting crystal growth by acting on thermodynamic parameters, such as pH and temperature, the supersaturation level, or by exploiting additives. Compounds containing carboxylic groups were found to reduce crystal growth in struvite (Kofina et al., 2007; Prywer et al., 2015; Polat and Sayan, 2020; Bayuseno et al., 2020). Between them, citric acid (CA) and citrates are of great interest also because of their biocompatibility (Mclean et al., 1990; Wang et al., 1993; Kofina et al., 2007; Perwitasari et al., 2017). During crystallization experiments, induction times and precipitation rates were found to be directly and inversely related to the concentration of the additive, respectively (Wang et al., 1993; Kofina et al., 2007; Prywer et al., 2015). Along with changes in crystal shape, both a reduction and an increase in crystal size have been reported (Wierzbicki et al., 1997; Kofina et al., 2007; Prywer et al., 2015). Such effects were related to complexing ability of citrate in solution and adsorption at the surface of growing nuclei and crystals.

A large body of literature is available for struvite, whereas much less efforts have been devoted to the isomorphic modification, struvite-K, despite its similar occurrence. Struvite-K is also of interest because it is a major phase in magnesium phosphate cements employed as bone substitute materials, in civil engineering as alternative to Portland cement, or as matrices for waste encapsulation (Wilson and Nicholson, 1993). Recent works pointed to CA as an effective and biocompatible additive for mitigating the fast reaction rates and excessive heat evolution during hardening (Wang et al., 2019; Wu et al., 2020). Nonetheless, there is insufficient information about its mechanism of action.

In this work, we have investigated the effect of the presence of citrate ion on the spontaneous precipitation of struvite-K from solution at room temperature and pH = 9, under different conditions of energy of mixing, concentrations of the reactants and additive.

Results from the time evolution of pH during the precipitation experiments, observation of obtained crystals with scanning electron microscopy (SEM), speciation analysis, concentration of CA in

solution, measurements of zeta potential (ξ), and X-ray photoelectron spectroscopy (XPS), allowed to propose a mechanism involving the intervention of ion complexation in solution and adsorption at the newly formed surfaces to explain the impact of CA on the rate of the precipitation reaction, the induction times, the amount of precipitate, the average size of crystals and crystal habit.

2. Experimental

2.1. Materials and methods

The precipitation of struvite-K was obtained by mixing two 25 mL solutions of $MgCl_2$ and KH_2PO_4 (KDP). Reagents were purchased from Merck and used as received. The deionized water was boiled before use in order to eliminate the effect of the dissolved CO_2 on the pH. The pH was brought to 9 by adding dropwise a 9M solution of NaOH and KOH to the $MgCl_2$ and KDP solutions, respectively. To investigate the effect of CA, the compound has been dissolved in the KDP solution before pH correction. The experiments were performed with a Metrohm 907 Titrando automatic mixing and titration unit (Metrohm, Switzerland), equipped with a pH probe and a thermal bath to ensure the attainment of the nominal temperature. The precipitation was monitored at 22 °C by continuous measurement of pH of the solution. Mixing was obtained by means of a magnetic stirrer operated at nominal speed 625 rpm and 375 rpm. The pH probe was calibrated before each experiment using ISO standard buffers.

For each stirring speed, the precipitation was obtained using two sets of solutions with Mg:K:P molar ratio 1:4:4: the first one containing 12.5 mM of Mg and 50 mM of K and P and the second one containing 25 mM of Mg and 100 mM of K and P. For each solution and stirring speed, the experiments were performed in the absence and in the presence of CA. The experimental plan is summarized in Table 1.

Table 1. Starting solutions employed in the precipitation experiments.

Sample identification	Mg mM	K mM	P mM	Citric acid mM
MKP_12.5_50_CA0	12.5	50	50	0
MKP_12.5_50_CA3	12.5	50	50	3
MKP_12.5_50_CA6	12.5	50	50	6
MKP_12.5_50_CA12	12.5	50	50	12
MKP_25_100_CA0	25	100	100	0
MKP_25_100_CA5	25	100	100	5
MKP_25_100_CA10	25	100	100	10
MKP_25_100_CA20	25	100	100	20

2.2.Materials characterization

The nature of the crystalline product was assessed with X-ray powder diffraction (XRPD) collecting spectra of the precipitate after filtration with isopropyl alcohol and drying overnight at 37 °C, by means of a Bruker D8 Advance diffractometer (Bruker AXS, USA). The Cu K_α wavelength was selected by means of a Ni filter and generated at 40 mA and 40 kV. Diffraction data were recorded in the angular range 5–70° 2θ with a virtual step scan of 0.0102° 2θ with 0.25 s/step counting time and spinning the sample at 15 rpm. After phase identification, the full profile fitting approach offered by the Rietveld method, implemented in the software TOPAS 4.2 (Bruker AXS, USA), was adopted to confirm the crystal structure.

Crystal size and morphology were observed with a Quanta 450 FEG (FEI, Czech Republic) scanning electron microscope operated at 20 kV accelerating voltage, 100 Pa pressure and adopting a gaseous backscatter electron detector, in order to limit the water loss from the samples. The crystals were dispersed on carbon adhesive tape and coated with a 10 nm thick gold film to minimize charging effects.

The amount of CA in solution after the precipitation experiments was determined by the spectrophotometric method based on Cu^{2+}–NH_3 complex decomposition by the citrate, as described elsewhere (Farajzadeh and Nagizadeh, 2002). The reagent blank Cu^{2+}–NH_3 complex solution was

employed to build a calibration curve (R^2 = 0.999) and perform the measurements of samples, by measuring absorbance at 600 and 750 nm. Details of the method and calibration results are available as Supplementary Material. The concentration of CA was measured on the samples obtained after the precipitation experiments with 25 mM of Mg and 100 mM of K and P, under fast stirring speed conditions, at the initial concentration of CA 5, 10, 20 and 30 mM. After 30 min, the experiment was considered concluded and the concentration of CA in the supernatant was measured after centrifugation for 10 min at 4000 rpm, with a spectrophotometer DR3900 (HACH, USA). Distribution diagrams of formed species were plotted using Hyperquad HYSS simulation and speciation software (Alderighi et al., 1999).

Zeta potential (ξ) of mineral particles was measured by dynamic light scattering by means of a Litesizer 500 instrument (Anton Paar, Austria). The measurements were performed at 25 °C, dispersing 0.1 wt.% of solid in water. Results were reported as average of 6 replicates.

X-ray photoelectron spectra (XPS) were collected adopting AlKα radiation (1486.6 eV) by means of a lab-based system (SPECS Surface Nano Analysis, GmbH), equipped with a multichannel electron energy analyser (Specs Phoibos 150) coupled with a differentially pumped electrostatic pre-lens system. Samples were pressed into a 0.5 mm thick indium foil (purity 99.99%). The core-level spectra of Mg 1*s*, O 1*s*, K 2*p*, C 1*s*, and P 2*p* were recorded with a pass energy of 20 eV, step size of 0.05 eV, and dwell time of 100 ms. The XPS signal was deconvoluted using Voigt-type function after background subtraction with KolXPD software.

3. Results and discussion

Fig. 1 illustrates the typical trend for the time-evolution of pH of the studied reactions. In the first minutes the pH drops sharply to gradually approach a plateau. Such behavior is compatible with the precipitation of the struvite family crystals (Babić-Ivančić et al., 2006). The latter is the dominant process, since CA is fully deprotonated in the range of pH of the experiment (see the distribution

diagram in the Supplementary Material Fig. S1). Under such conditions, a reaction, according to Eq. 1, proceeds, and, as has been shown for struvite crystallization experiments, the release of H^+ ions is related to the decrease in concentration of the Mg^{2+} ions and to the crystallization rate of the first struvite crystals formed (Bayuseno et al., 2020).

$$Mg^{2+} + K^+ + H_nPO_4^{n-3} + 6H_2O \rightarrow MgKPO_4 \cdot 6H_2O + nH^+ \quad (1)$$

In the range of pH observed during the experiment, the stable dominant form of phosphate is HPO_4^{2-}. Therefore, in Eq. 1 $n = 1$. The amount of Mg^{2+} ions subtracted from the solution is obtained from the pH change, as detailed in the Supplementary Material. This information can be used to derive an apparent rate of crystallization assuming a kinetic model for the process. A number of struvite crystallization experiments indicated that the process can be described with a first-order kinetic model (Ohlinger et al., 2000; Quintana et al., 2005; Bayuseno et al., 2020). Considering that struvite and struvite-K are isostructural, the same first-order equation was adopted to calculate the rate constant (k):

$$-\frac{dC}{dt} = k(C - C_{eq}) \quad (2)$$

Where C is the molar concentration of Mg^{2+} ions at any time t (min), C_{eq} is the molar concentration at equilibrium. An example of the nonlinear fit of the kinetic equation to the data is illustrated in Fig. 1, whereas the results are reported in Table 2.

When the precipitation in the absence of the additive is considered, an increase in the concentration of the reactants at the same starting pH led to an increase of the precipitation rates. This is related to the increase in supersaturation level (i.e. higher concentration of reactants) (Kofina et al., 2007; Rahaman et al., 2008). Higher rates are also observed increasing the mixing speed. In general, the rates are higher with respect to other experiments of struvite precipitation reported in the literature,

but lower respect to the results obtained in case of precipitation of struvite-K from synthetic urine at pH 9 (Zhang et al., 2018). Apart from the ionic strength of the solution, the higher supersaturation degree attained in the latter set of experiments is likely the main reason for this difference.

The effect of CA addition is apparent in the decrease of the overall precipitation rates and the delay in the onset of struvite-K crystallization. The nearly flat shape of the first part of the pH vs. time curve, indicating an induction time, is more marked at lower supersaturation levels. The length of the induction time increases with the amount of CA, a behaviour already observed during precipitation of struvite in presence of citrate (Kofina et al., 2007). Similarly, more effective mixing shortens the induction time (Ohlinger et al., 1999; Rahaman et al., 2008).

In struvite, the inhibiting effect of CA was attributed to adsorption at the surface of the growing crystals; a mechanism which has been considered the driving force for the morphological changes observed (Wierzbicki et al., 1997), although the measurement and simulation of chemical speciation indicated that complexation of cations in solution should also be involved (Prywer et al., 2015).

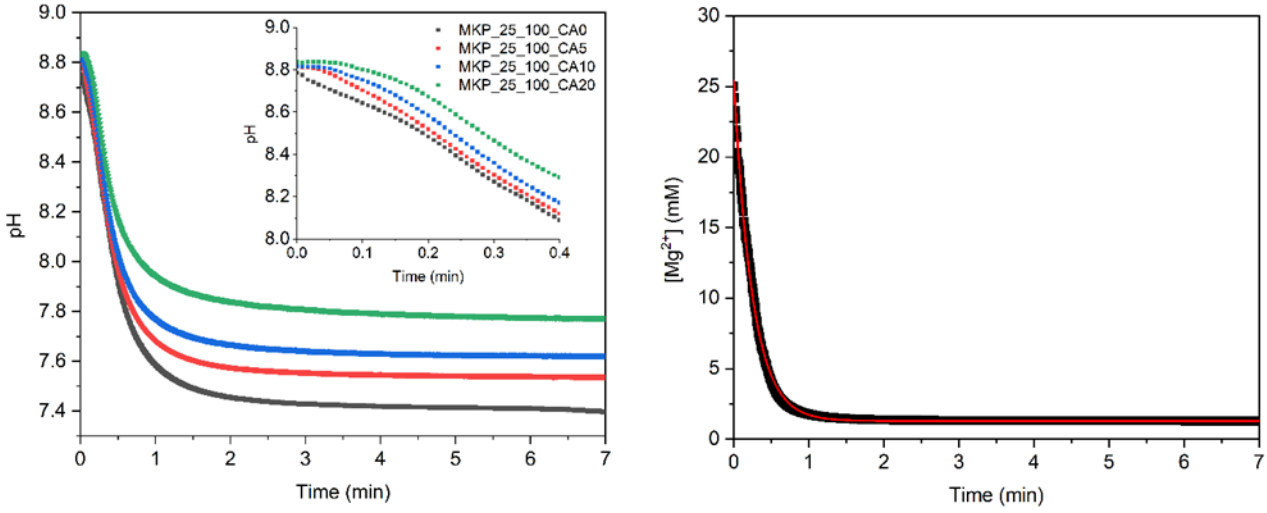

Figure 1. pH vs. time plots during the precipitation experiments at low stirring speed for the samples at different citric acid content (left). Example of nonlinear fit (red line) of the kinetic curve (black dots) of MKP_25_100_CA0 according to the first-order reaction model (right).

Table 2. Rate of the precipitation reaction with standard error of the nonlinear fit.

Sample	Slow stirring k / min^{-1}	R^2	Fast stirring k / min^{-1}	R^2
MKP_12.5_50_CA0	1.285±0.004	0.986	5.28±0.03	0.978
MKP_12.5_50_CA3	1.278±0.003	0.992	4.05±0.01	0.985
MKP_12.5_50_CA6	0.632±0.002	0.986	2.49±0.01	0.975
MKP_12.5_50_CA12	0.622±0.002	0.977	2.11±0.01	0.951
MKP_25_100_CA0	4.176±0.008	0.997	4.27±0.01	0.995
MKP_25_100_CA5	2.582±0.006	0.995	4.25±0.01	0.992
MKP_25_100_CA10	1.945±0.003	0.996	4.35±0.01	0.991
MKP_25_100_CA20	1.517±0.006	0.985	4.14±0.02	0.986

In all experiments, struvite-K was the only precipitate observed. An example of graphical output from the Rietveld refinement of XRPD spectrum of the precipitate, confirming the good agreement with the structure model of struvite-K, is reported as Supplementary Material Fig. S2.

Figs. 2 and 3 illustrate examples of the crystal morphology and size of the products as observed with SEM. When no CA was employed, at lower concentration of Mg, K and P reactants, the dominant crystal habit of struvite-K obtained during the experiment was prismatic, with maximum elongation along the *b*-axis; this shape is graphically rendered in Fig. 4. These morphologies have been frequently reported in the precipitation experiments of struvite (Wierzbicki et al., 1997; Prywer et al., 2015), which possesses the same space group symmetry. The needle-like morphology, obtained in some batch experiments aimed at precipitate struvite-K for nutrient recovery (Gao et al., 2018; Zhang et al., 2018), was not observed, most likely because of the less extreme hydrodynamic conditions of our tests. At the highest concentration of reactants, more prismatic individuals with dominant (001) faces joined together in a cockade (Fig. 3b, f-h); dendritic or X-shaped (twinned) crystals appeared (Fig. 3a, e). The latter morphology is also observed in struvite at high growth rates (Wang et al., 1993). In fact, these were the experiments exhibiting the highest rates (Table 2).

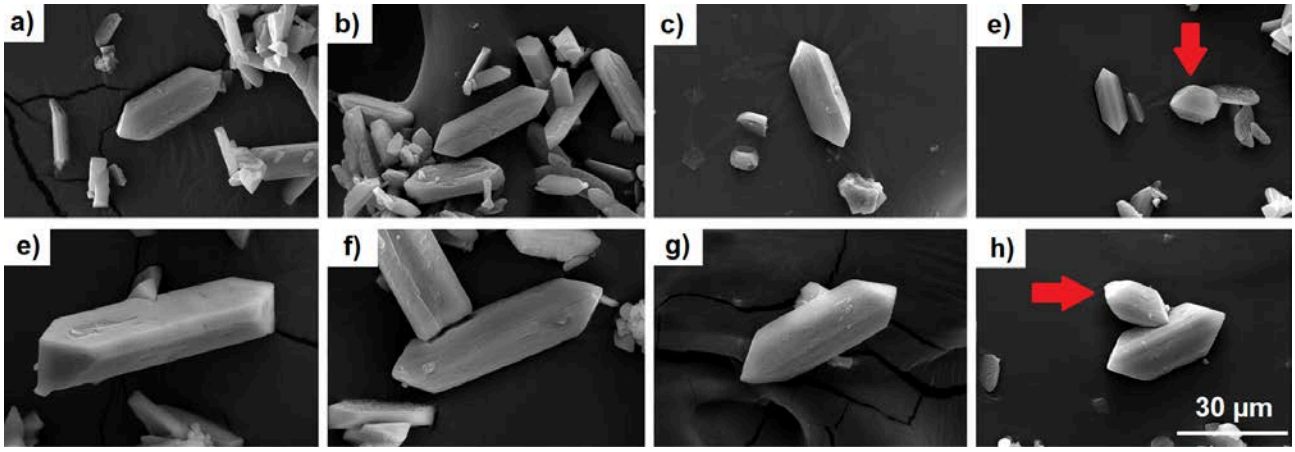

Figure 2. Gallery of SEM micrographs collected at same magnification for the struvite-K obtained increasing the concentration of CA at two stirring speeds. Low stirring speed: a-d, high stirring speed: e-h. MKP_12.5_50_CA0, a, e; MKP_12.5_50_CA3, b, f; MKP_12.5_50_CA6, c, g; MKP_12.5_50_CA12, d, h.

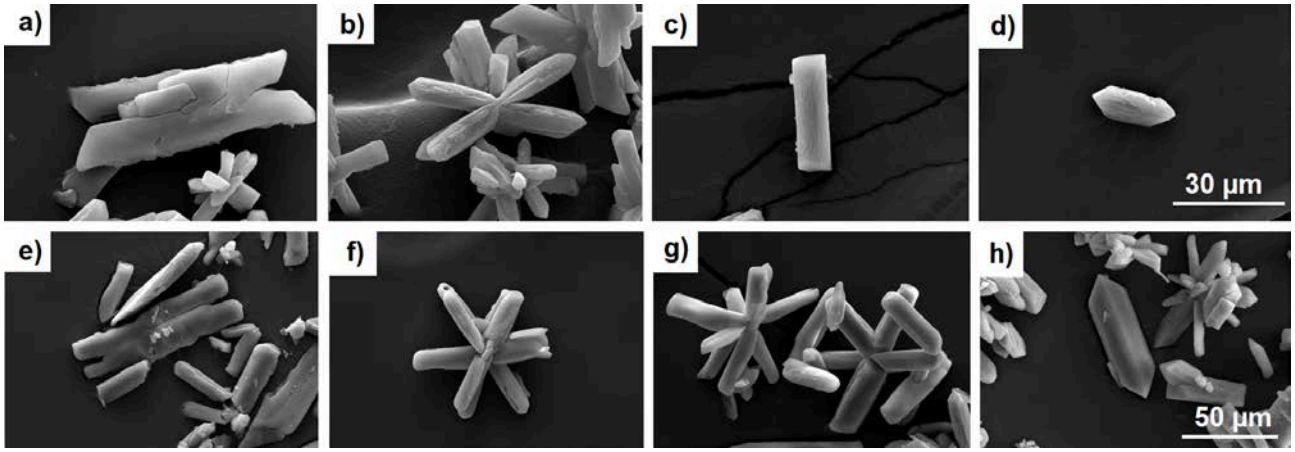

Figure 3 Gallery of SEM micrographs collected at same magnification for the struvite-K obtained increasing the concentration of CA at two stirring speeds. Low stirring speed (same magnification): a-d, high stirring speed (same magnification): e-h. MKP_25_100_CA0, a, e; MKP_25_100_CA5, b, f; MKP_25_100_CA10, c, g; MKP_25_100_CA20, d, h.

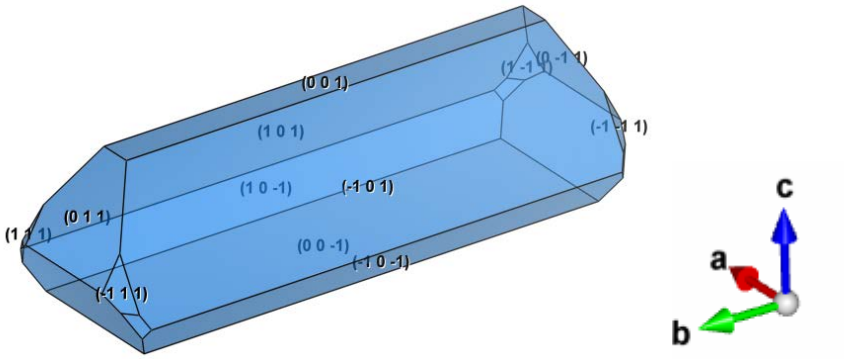

Figure 4. Schematic representation of the common crystal habit of struvite-K crystals with some of the faces indexed.

The gradual addition of CA induced changes in crystal morphology and size. The average size of the precipitated crystals appeared inversely related to the concentration of CA (see Fig. 2 and 3, a-d and e-h), indicating a strong inhibiting effect of CA on crystal growth. At the same time, CA seems to reduce crystal elongation, resulting in individuals relatively larger along the *a*-axis and shorter along the *b*-axis. Reduction in size and alteration of crystal shape have been described upon addition of citrates or compounds containing carboxylic groups during the precipitation of Ca-phosphates (Tenhuisen and Brown, 1994; Bohner et al., 1996; López-Macipe et al., 1998; Fukuda et al., 2017) and struvite (Kofina et al., 2007; Prywer et al., 2015; Perwitasari et al., 2017; Polat and Sayan, 2020). However, few papers reported on detailed morphological studies. An arrow head morphology, dominated by (101) and ($\bar{1}$01) faces, with (001) face virtually not expressed, was documented for struvite growing in the presence of phosphocitrate (Wierzbicki et al., 1997). Conversely, in the presence of sodium citrate, the (012) face was suppressed and the (001) face was progressively more expressed (Prywer et al., 2015). Such effects were related to the interaction at the molecular level between the additive and the crystal surfaces, that is, selective adsorption at crystal faces. In our precipitation experiments, at the lower concentration of the reactants Mg, K and P, the increase in CA content essentially brought about the decrease in crystal elongation ((001) face

more expressed) and size mentioned above. Occasionally, a coffin-lid habit, missing the (001) face, was also observed (Fig. 4d and h, red arrows). In a similar fashion, at high concentration of reactants, the crystal shape (mostly prismatic with more expressed (001) face terminated by (101) and ($\bar{1}$01) faces) is preserved irrespective of the increase in the concentration of CA and only the size of crystals is reduced. It is worth noting that formation of large (001) faces was also observed during the spontaneous precipitation of struvite, when fast crystallization kinetics are attained (Abbona and Boistelle, 1979), which is the case of our experiments at higher concentration of reactants (Fig. 3). Therefore, it can be inferred that in our experiments, the conditions of synthesis, and especially the degree of supersaturation, influence the crystal habit, and CA emphasizes the character of the crystal form, mostly enhancing the expression of the (001) face. Adsorption of an inhibitor at specific crystal faces leads to the enhanced expression of such faces, because their relative growth rate is decreased. It is thus proposed that the modifications in struvite-K morphology may be explained by preferential binding of citric acid at the (001) face, thanks to the residual negative charge of the molecule. A similar mechanism was invoked to explain the habit of struvite growing in the presence of sodium citrate (Prywer et al., 2015).

The complexing ability of citrate ion in solution and its adsorption behaviour will be now considered in turn with reference to the precipitation of struvite-K.

According to the dissociation constants of CA and the distribution of species as a function of pH and temperature, in the pH interval 7.5−9, covered during our experiments, the dominant form of citrate in solution is the fully deprotonated ion Cit^{3-} (López-Macipe et al., 1998).

With respect to Mg^{2+} ions, the following equilibria are therefore established:

$$Mg^{2+} + Cit^{3-} \rightleftarrows MgCit^{-} \quad (3)$$

$$H^{+} + OH^{-} \rightleftarrows H_2O \quad (4)$$

Similar equations hold for potassium ion (Zelenina and Zelenin, 2005).

Although the complexation in solution depends also on ionic strength and pH (which affect the thermodynamic stability constant of the complexes (Piispanen and Lajunen, 1995; Wyrzykowski et al., 2010)), as a general rule, the stability is much higher for Mg complexes than for K ones (Blaquiere and Berthon, 1987; Zelenina and Zelenin, 2005). Simulation of distribution diagrams confirmed that at pH >7 a large part of Mg is in the form of the $MgCit^-$ complex (Fig.5 and Supplementary Material Fig. S3), in analogy with previous results from crystallization of struvite (Prywer et al., 2015). Likewise, complex formation in solution may be invoked to explain the inhibiting effect of CA on crystallization of struvite-K because of the progressive decrease in apparent concentration of Mg^{2+} ion increasing the amount of the additive.

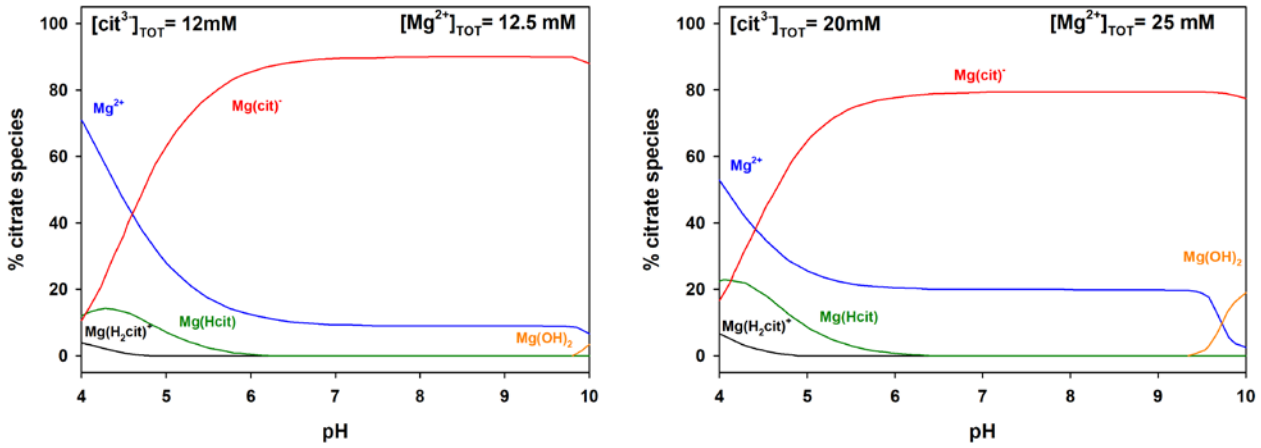

Figure 5. Relative amount of magnesium complexes as a function of pH at two concentrations of Mg ions and CA.

As mentioned in the foregoing discussion, CA may also interfere with the crystallization process through surface adsorption. This mechanism has been found to control the crystallization of Ca-carbonate, hindering crystal growth (Wada et al., 2001; Reddy and Hoch, 2001), or impairing the formation of nuclei of critical size (Westin and Rasmuson, 2005). Similarly, during the synthesis of Ca-phosphates, the decrease in crystal size and modifications of crystal habit were attributed to citrate adsorption at crystal surface (Tenhuisen and Brown, 1994; Sarda et al., 2002). It is well-

documented that upon adsorption of the negatively charged carboxylate ion (COO^-), the mineral surface exhibits more negative values of zeta potential (Kallay and Matijevic, 1985; Mudunkotuwa and Grassian, 2010). The results obtained from our samples were: −13.1±1.0 mV and −16.2±0.4 mV for MKP_25_100_CA0 and MKP_25_100_CA20 precipitated at low stirring speed, respectively, substantiating the view that CA is adsorbed on struvite-K. Such mechanism was confirmed by the measurement of the amount of CA left in solution after the precipitation experiments of MKP_25_100. As reported in Table 3, the citrate is effectively subtracted from the solution, indicating its adsorption on the crystal surface. The amounts are in general agreement with those reported for Na-citrate adsorbed at hydroxyapatite (López-Macipe et al., 1998). These results also show that, along with the reduced average crystal size, the total amount of precipitated struvite-K decreases with increasing the amount of additive. The eventuality of incorporation of CA into the crystal structure of struvite-K seems unlikely, given the big size of the molecule. All in all, the evidence of the presence of citrate into the crystal structure of precipitated carbonates or phosphates are not conclusive (Tobler et al., 2015; Chatzipanagis et al., 2016), whereas, in such systems, surface adsorption effect was recognized to retard nucleation, yielding smaller crystals and lower amount of precipitate (Tobler et al., 2015).

Table 3. Amount of precipitated struvite-K, initial (*C0*) and equilibrium (C_{eq}) concentration of citric acid in the series of samples MKP_25_100 precipitated at low stirring speed.

struvite-K	C_0	C_{eq}
g	mM	mM
0.1577	0	-
0.1417	5	3.49
0.1178	10	6.48
0.0652	20	15.03
0.0208	30	24.51

Being a highly surface-sensitive technique, XPS may provide further insights into the nature of the interaction of CA with the mineral surface. The background subtracted XPS spectra and the binding energy (BE) components, obtained through signal deconvolution, are illustrated in Fig. 6; the results of the analysis are summarized in Table 4. The phosphorus BE P 2*p*, provided as Supplementary Material Fig. S4, was found to be 132.8 eV in MKP_25_100_CA0 and 132.7 eV in MKP_25_100_CA20. These values are ascribed to the P=O bonds, in line with BE measured in struvite (Polat and Sayan, 2020).

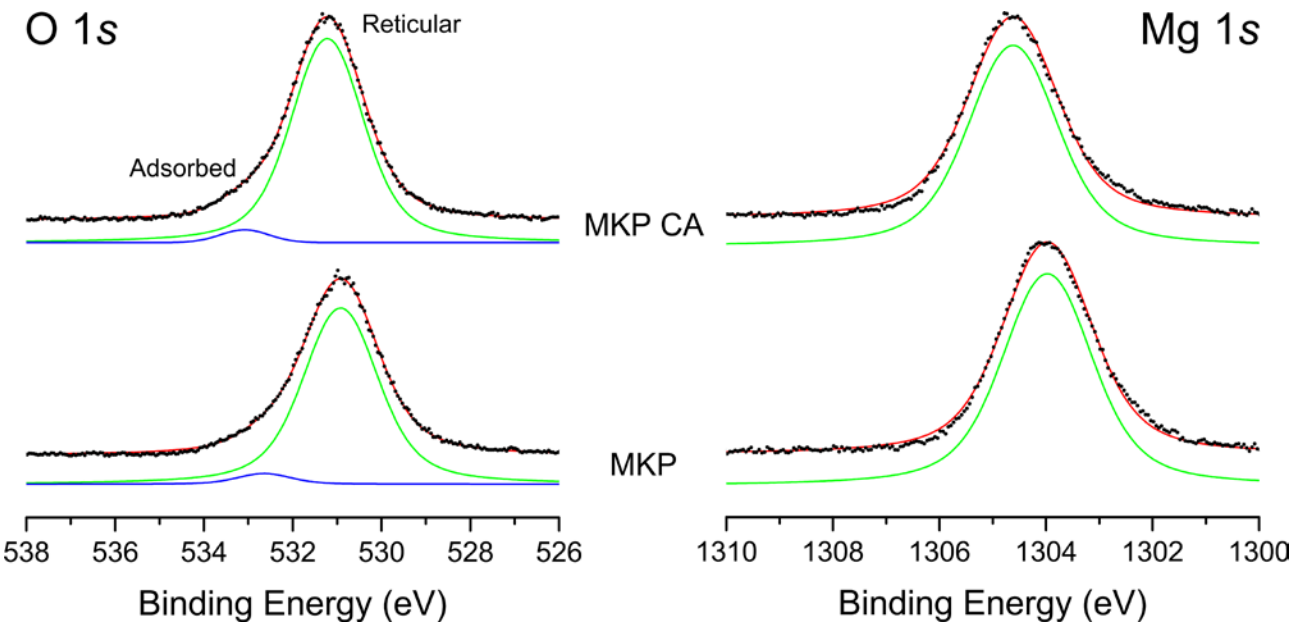

Figure 6. Background subtracted XPS spectra from the investigated samples with results of signal deconvolution (continuous red line). Components are displaced vertically for the sake of clarity.

The interpretation of the O 1*s* signal is hampered by the overlap of broad components in a narrow range of BE. The main peak was disentangled into two components; one at 530.9 eV, assigned to oxygen in the struvite-K, and one at 532.6 eV, attributed to oxygen from adsorbed species (Ardizzone et al., 1997). In the sample synthesized in the presence of CA, the signal is, in complex, slightly broader, and BE increases to 531.2 eV in the component accounting for reticular oxygen,

and to 533.1 eV in the one related to the adsorbed species. This is in agreement with the effect of surface adsorption of citrate, as previously observed in struvite prepared in the presence of carboxylic acids (Polat and Sayan, 2020). In previous studies on struvite synthesized in the presence of additives containing carboxylic groups, Mg was considered the target of the adsorption processes. In agreement with this view, the BE of Mg 2*p* increases of 0.6 eV in the sample synthesized in the presence of CA.

As illustrated in Supplementary Material Fig. S4, compared to struvite, in K-struvite, the analysis of the region of C 1*s* BE is further complicated by severe peak overlap with the signal from K $2p_{3/2}$ BE at 292.8 eV (Moulder et al., 1992). The –O–C=O component ascribed to carboxylic groups, diagnostic of the interaction of the mineral surface with CA, is detected at BE > 288 eV (Frydman et al., 1997; Wei et al., 2019). This means that this tiny C 1*s* signal falls under the high intensity K $2p_{3/2}$ peak, preventing from its accurate quantification.

Table 4. Results of XPS analysis of the investigated samples.

Sample		O 1s	Mg 1s	P 2p
MKP_25_100_CA0	530.9	532.6	1304.0	132.8
MKP_25_100_CA20	531.2	533.1	1304.6	132.7

The results presented so far indicate that the reaction rate during precipitation of struvite-K from solution without additive can be satisfactorily described with a first-order kinetic model. The reaction is accelerated by increasing the mixing energy and the supersaturation degree. CA seems to interfere with the precipitation reaction by exploiting complexing ability in solution (lowering the activity of the ions, with large prevalence for Mg^{2+}) and be adsorbed at the surface of the forming solid. The complex interplay between these processes results in a decrease of the apparent rates, a reduction in average crystal size and in the amount of precipitated product when the content of CA

increases. The reaction path is also affected, as evidenced by the decrease in the R^2 values of the fit increasing the content in CA. Similar results were obtained when precipitating struvite in the presence of carboxylic groups (Perwitasari et al., 2017; Bayuseno et al., 2020). This indicates that the single-step first-order reaction model is insufficient to describe the system, and more advanced approaches, which are outside the scope of the present work, are required.

When the influence of CA adsorption on crystal nucleation and growth is concerned, thermodynamic parameters, such as interfacial energy, are often only indicative of the role of additives, since they reflect average values from different surfaces possessing complex structure and not necessarily in equilibrium, especially during nucleation (Westin and Rasmuson, 2005). In this scenario, during precipitation of struvite-K, citrate adsorption may be thought to occur in the nucleation stage and/or, as proposed for Ca-carbonate and Ca-phosphate systems, as early as in the pre-nucleation stage, by hindering the integration of lattice ions, impairing the formation of nuclei of critical size (Westin and Rasmuson, 2005; Chatzipanagis et al., 2016). When critical nuclei are formed, the growth of crystals is influenced by the selective adsorption of CA on the different crystal faces, in reason of their different affinity for the additive.

4. Conclusions

Precipitation of struvite-K from solution has been studied in the presence of citric acid at room temperature and pH 9, under different concentrations of the reactants and stirring speeds.

- The apparent rates of struvite-K precipitation were reduced in the presence of the additive with respect to the control. As for the control, the rates decreased decreasing stirring speed and reactant concentration.
- Under all conditions, the additive increased induction time with respect to the control. The extent of this effect was directly related to the amount of the additive and inversely related to the intensity of mixing and concentration of reactants.

- Citric acid caused a reduction in the total amount of precipitate with respect to the control. The extent of this effect was directly related to the amount of additive, in analogy with other experiments conducted on struvite, Ca-carbonate and Ca-phosphate.
- Formation of citrate complexes, with $MgCit^-$ by far the most represented under the conditions of the experiments, is thought to be an inhibiting factor, contributing to the increase in induction times and decrease in the total amount of precipitate.
- Adsorption of citric acid at the surface of the growing nuclei, and, perhaps, of pre-nucleation clusters, as well as at the crystal faces, is also occurring, and exerts control on the size and shape of the growing crystals.
- According to the modifications induced by CA on the crystal habit of struvite-K, it is proposed that the additive strongly binds to the (001) faces.

Acknowledgments

The authors acknowledge support from the Czech Science Foundation GA ČR (Grant Number 20-01280S), the Czech Academy of Sciences, Institute of Theoretical and Applied Mechanics (RVO 68378297), and the CERIC-ERIC Consortium for the access to the XPS experimental facility. The authors also wish to thank Irena Adámková for the kinetic analysis.

References

Abbona F. and Boistelle R. (1979) Growth morphology and crystal habit of struvite crystals (MgNH4PO4 · 6 H2O). *J. Cryst. Growth* **46**, 339–354. Available at: https://linkinghub.elsevier.com/retrieve/pii/0022024879900824.

Alderighi L., Gans P., Ienco A., Peters D., Sabatini A. and Vacca A. (1999) Hyperquad simulation and speciation (HySS): a utility program for the investigation of equilibria involving soluble and partially soluble species. *Coord. Chem. Rev.* **184**, 311–318. Available at: https://linkinghub.elsevier.com/retrieve/pii/S0010854598002604.

Ardizzone S., Bianchi C. L., Fadoni M. and Vercelli B. (1997) Magnesium salts and oxide: an XPS overview. *Appl. Surf. Sci.* **119**, 253–259. Available at: https://linkinghub.elsevier.com/retrieve/pii/S0169433297001803.

Babić-Ivančić V., Kontrec J., Brečević L. and Kralj D. (2006) Kinetics of struvite to newberyite

transformation in the precipitation system MgCl2–NH4H2PO4–NaOH–H2O. *Water Res.* **40**, 3447–3455. Available at: https://linkinghub.elsevier.com/retrieve/pii/S0043135406004362.

Bayuseno A. P., Perwitasari D. S., Muryanto S., Tauviqirrahman M. and Jamari J. (2020) Kinetics and morphological characteristics of struvite (MgNH4PO4.6H2O) under the influence of maleic acid. *Heliyon* **6**, e03533. Available at: https://linkinghub.elsevier.com/retrieve/pii/S2405844020303789.

Blaquiere C. and Berthon G. (1987) Speciation studies in relation to magnesium bioavailability. Formation of Mg(II) complexes with glutamate, aspartate, glycinate, lactate, pyroglutamate, pyridoxine and citrate, and appraisal of their potential significance towards magnesium gastrointestin. *Inorganica Chim. Acta* **135**, 179–189.

Bohner M., Lemaitre J. and Ring T. A. (1996) Effects of Sulfate, Pyrophosphate, and Citrate Ions on the Physicochemical Properties of Cements Made of beta-Tricalcium Phosphate-Phosphoric Acid-Water Mixtures. *J. Am. Ceram. Soc.* **79**, 1427–1434. Available at: http://doi.wiley.com/10.1111/j.1151-2916.1996.tb08746.x.

Chatzipanagis K., Iafisco M., Roncal-Herrero T., Bilton M., Tampieri A., Kröger R. and Delgado-López J. M. (2016) Crystallization of citrate-stabilized amorphous calcium phosphate to nanocrystalline apatite: a surface-mediated transformation. *CrystEngComm* **18**, 3170–3173. Available at: http://xlink.rsc.org/?DOI=C6CE00521G.

Farajzadeh M. A. and Nagizadeh S. (2002) Citric Acid Determination by Dual Wavelength Spectrophotometry. *J. Chinese Chem. Soc.* **49**, 619–624. Available at: https://onlinelibrary.wiley.com/doi/10.1002/jccs.200200095.

Frydman E., Cohen H., Maoz R. and Sagiv J. (1997) Monolayer Damage in XPS Measurements As Evaluated by Independent Methods. *Langmuir* **13**, 5089–5106. Available at: https://pubs.acs.org/doi/10.1021/la962058q.

Fukuda N., Tsuru K., Mori Y. and Ishikawa K. (2017) Effect of citric acid on setting reaction and tissue response to β -TCP granular cement. *Biomed. Mater.* **12**, 015027. Available at: https://iopscience.iop.org/article/10.1088/1748-605X/aa5aea.

Gao Y., Liang B., Chen H. and Yin P. (2018) An experimental study on the recovery of potassium (K) and phosphorous (P) from synthetic urine by crystallization of magnesium potassium phosphate. *Chem. Eng. J.* **337**, 19–29. Available at: https://linkinghub.elsevier.com/retrieve/pii/S138589471732199X.

Kallay N. and Matijevic E. (1985) Adsorption at solid/solution interfaces. 1. Interpretation of surface complexation of oxalic and citric acids with hematite. *Langmuir* **1**, 195–201. Available at: https://pubs.acs.org/doi/abs/10.1021/la00062a003.

Kofina A. N., Demadis K. D. and Koutsoukos P. G. (2007) The Effect of Citrate and Phosphocitrate On Struvite Spontaneous Precipitation. *Cryst. Growth Des.* **7**, 2705–2712. Available at: https://pubs.acs.org/doi/10.1021/cg0603927.

López-Macipe A., Gómez-Morales J. and Rodríguez-Clemente R. (1998) The Role of pH in the Adsorption of Citrate Ions on Hydroxyapatite. *J. Colloid Interface Sci.* **200**, 114–120. Available at: https://linkinghub.elsevier.com/retrieve/pii/S0021979797953431.

Mclean R. J. C., Downey J., Clapham L. and Nickel J. C. (1990) Influence of Chondroitin Sulfate, Heparin Sulfate, and Citrate on Proteus Mirabilis-Induced Struvite Crystallization in Vitro. *J. Urol.* **144**, 1267–1271. Available at: http://www.jurology.com/doi/10.1016/S0022-5347%2817%2939717-3.

Mclean R. J. C., Nickel J. C., Cheng K. J., Costerton J. W. and Banwell J. G. (1988) The ecology

and pathogenicity of urease-producing bacteria in the urinary tract. *Crit. Rev. Microbiol.* **16**, 37–79.

Mohajit, Bhattarai K. K., Taiganides E. P. and Yap B. C. (1989) Struvite deposits in pipes and aerators. *Biol. Wastes* **30**, 133–147. Available at: https://linkinghub.elsevier.com/retrieve/pii/0269748389900670.

Moulder J. F., Stickle W. F., Sobol P. E. and Bomben K. D. (1992) *Handbook of X-ray photoelectron spectroscopy: a reference book of standard spectra for identification and interpretation of XPS data*., Available at: https://www.cnyn.unam.mx/~wencel/XPS/MANXPS.pdf.

Mudunkotuwa I. A. and Grassian V. H. (2010) Citric Acid Adsorption on TiO 2 Nanoparticles in Aqueous Suspensions at Acidic and Circumneutral pH: Surface Coverage, Surface Speciation, and Its Impact on Nanoparticle−Nanoparticle Interactions. *J. Am. Chem. Soc.* **132**, 14986–14994. Available at: https://pubs.acs.org/doi/10.1021/ja106091q.

Ohlinger K. N., P.E., Young T. M. and Schroeder E. D. (1999) Kinetics Effects on Preferential Struvite Accumulation in Wastewater. *J. Environ. Eng.* **125**, 730–737. Available at: http://ascelibrary.org/doi/10.1061/%28ASCE%290733-9372%281999%29125%3A8%28730%29.

Ohlinger K. N., Young T. M. and Schroeder E. D. (2000) Postdigestion Struvite Precipitation Using a Fluidized Bed Reactor. *J. Environ. Eng.* **126**, 361–368. Available at: http://ascelibrary.org/doi/10.1061/%28ASCE%290733-9372%282000%29126%3A4%28361%29.

Perwitasari D. S., Edahwati L., Sutiyono S., Muryanto S., Jamari J. and Bayuseno A. P. (2017) Phosphate recovery through struvite-family crystals precipitated in the presence of citric acid: mineralogical phase and morphology evaluation. *Environ. Technol.* **38**, 2844–2855. Available at: https://www.tandfonline.com/doi/full/10.1080/09593330.2017.1278795.

Piispanen J. and Lajunen L. H. J. (1995) Complex formation equilibria of some aliphatic a-hydroxycarboxylic acids. *Acta Chem. Scand.* **49**, 235–240.

Polat S. and Sayan P. (2020) Preparation, characterization and kinetic evaluation of struvite in various carboxylic acids. *J. Cryst. Growth* **531**, 125339. Available at: https://linkinghub.elsevier.com/retrieve/pii/S0022024819305548.

Prywer J., Mielniczek-Brzóska E. and Olszynski M. (2015) Struvite crystal growth inhibition by trisodium citrate and the formation of chemical complexes in growth solution. *J. Cryst. Growth* **418**, 92–101. Available at: https://linkinghub.elsevier.com/retrieve/pii/S0022024815001177.

Quintana M., Sánchez E., Colmenarejo M. F., Barrera J., García G. and Borja R. (2005) Kinetics of phosphorus removal and struvite formation by the utilization of by-product of magnesium oxide production. *Chem. Eng. J.* **111**, 45–52. Available at: https://linkinghub.elsevier.com/retrieve/pii/S1385894705001919.

Rahaman M. S., Ellis N. and Mavinic D. S. (2008) Effects of various process parameters on struvite precipitation kinetics and subsequent determination of rate constants. *Water Sci. Technol.* **57**, 647–654. Available at: https://iwaponline.com/wst/article/57/5/647/14058/Effects-of-various-process-parameters-on-struvite.

Reddy M. M. and Hoch A. R. (2001) Calcite Crystal Growth Rate Inhibition by Polycarboxylic Acids. *J. Colloid Interface Sci.* **235**, 365–370. Available at: https://linkinghub.elsevier.com/retrieve/pii/S0021979700973788.

Sarda S., Fernández E., Nilsson M., Balcells M. and Planell J. A. (2002) Kinetic study of citric acid

influence on calcium phosphate bone cements as water-reducing agent. *J. Biomed. Mater. Res.* **61**, 653–659. Available at: http://doi.wiley.com/10.1002/jbm.10264.

Schmidt M. and Steinemann S. G. (1991) XPS studies of amino acids adsorbed on titanium dioxide surfaces. *Fresenius. J. Anal. Chem.* **341**, 412–415. Available at: http://link.springer.com/10.1007/BF00321947.

Shaddel S., Grini T., Andreassen J.-P., Østerhus S. W. and Ucar S. (2020) Crystallization kinetics and growth of struvite crystals by seawater versus magnesium chloride as magnesium source: towards enhancing sustainability and economics of struvite crystallization. *Chemosphere* **256**, 126968. Available at: https://linkinghub.elsevier.com/retrieve/pii/S0045653520311619.

Tenhuisen K. S. and Brown P. W. (1994) The effects of citric and acetic acids on the formation of calcium-deficient hydroxyapatite at 38 C. *J. Mater. Sci. Mater. Med.* **5**, 291–298. Available at: http://link.springer.com/10.1007/BF00122399.

Tobler D. J., Rodriguez-Blanco J. D., Dideriksen K., Bovet N., Sand K. K. and Stipp S. L. S. (2015) Citrate Effects on Amorphous Calcium Carbonate (ACC) Structure, Stability, and Crystallization. *Adv. Funct. Mater.* **25**, 3081–3090. Available at: https://onlinelibrary.wiley.com/doi/10.1002/adfm.201500400.

Wada N., Kanamura K. and Umegaki T. (2001) Effects of Carboxylic Acids on the Crystallization of Calcium Carbonate. *J. Colloid Interface Sci.* **233**, 65–72. Available at: https://linkinghub.elsevier.com/retrieve/pii/S0021979700972151.

Wang S., Xu C., Yu S., Wu X., Jie Z. and Dai H. (2019) Citric acid enhances the physical properties, cytocompatibility and osteogenesis of magnesium calcium phosphate cement. *J. Mech. Behav. Biomed. Mater.* **94**, 42–50. Available at: https://linkinghub.elsevier.com/retrieve/pii/S1751616118316874.

Wang Y., Grenabo L., Hedelin H., McLean R. J. C., Curtis Nickel J. and Pettersson S. (1993) Citrate and urease-induced crystallization in synthetic and human urine. *Urol. Res.* **21**, 109–115. Available at: http://link.springer.com/10.1007/BF01788828.

Wei L., Hong T., Li X., Li M., Zhang Q. and Chen T. (2019) New insights into the adsorption behavior and mechanism of alginic acid onto struvite crystals. *Chem. Eng. J.* **358**, 1074–1082. Available at: https://linkinghub.elsevier.com/retrieve/pii/S138589471832062X.

Westin K.-J. and Rasmuson Å. C. (2005) Nucleation of calcium carbonate in presence of citric acid, DTPA, EDTA and pyromellitic acid. *J. Colloid Interface Sci.* **282**, 370–379. Available at: https://linkinghub.elsevier.com/retrieve/pii/S0021979704010021.

Wierzbicki A., Sallis J. D., Stevens E. D., Smith M. and Sikes C. S. (1997) Crystal Growth and Molecular Modeling Studies of Inhibition of Struvite by Phosphocitrate. *Calcif. Tissue Int.* **61**, 216–222. Available at: http://link.springer.com/10.1007/s002239900326.

Wilson A. and Nicholson J. W. (1993) *Acid-base cements*., Cambridge University Press.

Wu X., Dai H., Yu S., Zhao Y., Long Y., Li W. and Tu J. (2020) Magnesium Calcium Phosphate Cement Incorporating Citrate for Vascularized Bone Regeneration. *ACS Biomater. Sci. Eng.*, acsbiomaterials.0c00929. Available at: https://pubs.acs.org/doi/10.1021/acsbiomaterials.0c00929.

Wyrzykowski D., Czupryniak J., Ossowski T. and Chmurzyński L. (2010) Thermodynamic interactions of the alkaline earth metal ions with citric acid. *J. Therm. Anal. Calorim.* **102**, 149–154. Available at: http://link.springer.com/10.1007/s10973-010-0970-y.

Zelenina T. E. and Zelenin O. Y. (2005) Complexation of citric and tartaric acids with Na and K ions in aqueous solution. *Koord. Khimiya* **31**, 253–261.

Zhang C., Xu K., Zheng M., Li J. and Wang C. (2018) Factors Affecting the Crystal Size of Struvite-K Formed in Synthetic Urine Using a Stirred Reactor. *Ind. Eng. Chem. Res.* **57**, 17301–17309. Available at: https://pubs.acs.org/doi/10.1021/acs.iecr.8b03328.